INORGANIC CHEMISTRY FRONTIERS

RESEARCH ARTICLE

View Article Online
View Journal | View Issue

Cite this: *Inorg. Chem. Front.*, 2025, **12**, 3449

Guest-induced gate-opening in a flexible MOF adsorbent that exhibits benzene/cyclohexane selectivity†

Guo-Ao Li,‡[a] Min Deng,‡[a] Wei Guo,[a] Shuang Yin,[a] Yan-E Liu,[a] Ai-Xin Zhu *[a] and Michael J. Zaworotko *[b]

Received 24th January 2025,
Accepted 6th March 2025

DOI: 10.1039/d5qi00261c

rsc.li/frontiers-inorganic

We report the synthesis of a 2-fold interpenetrated primitive cubic (**pcu**) topology network, **X-pcu-11-Zn**, formulated as $[Zn_2(DMTDC)_2(dpb)]$ (H_2DMTDC = 3,4-dimethylthieno[2,3-*b*]thiophene-2,5-dicarboxylic acid; dpb = 1,4-di(pyridin-4-yl)benzene). Upon removal of solvent molecules from the as-synthesised form, **X-pcu-11-Zn-α**, transformation from a large-pore "open" phase to a narrow pore phase, **X-pcu-11-Zn-β**, occurred. The β-phase subsequently exhibited guest-induced switching as evidenced by a 2-step type F-IV[2] adsorption isotherm for N_2 at 77 K and a 3-step profile with two gate-opening pressures for CO_2 at 195 K. Dynamic vapour sorption studies revealed selective sorption of methanol, ethanol, and CH_3CN over H_2O at 298 K. Furthermore, **X-pcu-11-Zn-β** selectively adsorbed benzene over cyclohexane concomitant with a gate-opening effect driven by structural transformations. Importantly, the transformations between the guest-free and guest-loaded structures were found to be reversible over six adsorption/desorption cycles. Single-crystal X-ray diffraction analysis of the benzene-loaded phase indicates that selective benzene binding can be attributed to π–π and C–H···π aromatic packing interactions.

Introduction

Metal–organic frameworks (MOFs)[1] or porous coordination polymers (PCPs)[2] are an evolving class of porous materials that are of interest for key commodity separations, especially for difficult-to-separate hydrocarbons.[3] Flexible MOFs (FMOFs), a subset of MOFs, are stimuli-responsive soft porous crystalline solids that undergo structural transformations in response to external stimuli such as pressure, heat, light, cation/anion exchange, or guest (gas/vapour/solvent) uptake/removal.[4–7] FMOFs are characterised by atypical stepped or "S-shaped" isotherms that are concomitant with gate-opening phenomena. Hysteresis can be associated with these breathing or swelling processes.[8,9] These stimuli-responsive structural transformations can result in useful properties in the context of gas storage and separation,[10,11] guest capture and release,[12] and molecular sensing,[13–15] in some cases setting benchmark performance.[16]

Separation of benzene (Bz) and cyclohexane (Cy) is a challenge for the chemical and petrochemical industries. Cy is primarily obtained through the catalytic hydrogenation of Bz and unreacted Bz must be removed from the reactor's effluent stream to generate high-purity Cy. However, this separation is challenging due to their similar boiling points (Bz, 80.1 °C; Cy, 80.7 °C), molecular geometries (Bz, 3.3 × 6.6 × 7.3 Å^3; Cy, 5.0 × 6.6 × 7.2 Å^3), and Lennard–Jones collision diameters.[17,18] The similar boiling points and the formation of azeotropes render distillation processes poorly effective. Currently, the predominant industrial methods for separating Bz/Cy mixtures are extractive distillation and azeotropic distillation, both of which have high energy footprints and are accompanied by process complexity and high operating costs.[19–21] It is therefore desirable to develop separation methods that are easier and more energy-efficient for the separation of Bz and Cy. A similar challenge exists for alcohol/water separations.

To enable selective separation between sorbates with similar physicochemical properties, the development of physisorbents with tight binding sites has proven to be fruitful as exemplified by CO_2 and C_2H_2 selective adsorbents.[22,23] For Bz/Cy, π–π, H-π, and H-bonding interactions are likely to drive selective Bz binding and could also induce structural transformations.[24–29] FMOFs comprised of aromatic linker

[a]*Key Laboratory of Modern Separation Analysis and Substance Transformation, Faculty of Chemistry and Chemical Engineering, Yunnan Normal University, Kunming 650500, China. E-mail: zaxchem@126.com*
[b]*Department of Chemical Sciences, Bernal Institute, University of Limerick, Limerick V94T9PX, Ireland. E-mail: xtal@ul.ie*

†Electronic supplementary information (ESI) available: Experimental details, single-crystal XRD data, PXRD patterns, IR spectra, TGA curves, *etc.* CCDC 2372920–2372922. For ESI and crystallographic data in CIF or other electronic format see DOI: https://doi.org/10.1039/d5qi00261c

‡These authors contributed equally to this work.

ligands would be expected to offer suitable pore chemistry for Bz binding and, because of inherent flexibility, offer the possibility of induced-fit binding for Bz that is reminiscent of enzyme–substrate binding.[26–29] This principle was demonstrated by Kitagawa's group in an FMOF featuring a flexible undulating channel that exhibited selective adsorption of Bz over Cy *via* gate-opening triggered by CH-π interactions.[26] Chen *et al.* reported a flexible MOF with a similar mechanism for selective adsorption of Bz,[27] whereas Ghosh *et al.* reported an FMOF with a π-electron deficient ligand that exhibited Bz/Cy recognition and structural transformation induced by Bz.[28]

In this study, we report a new 2-fold interpenetrated FMOF, $[Zn_2(DMTDC)_2(dpb)]$ (**X-pcu-11-Zn**), comprising two aromatic π-conjugated ligands (Scheme 1): 3,4-dimethylthieno[2,3-*b*]thiophene-2,5-dicarboxylic acid (H_2DMTDC) and 1,4-di(pyridin-4-yl)benzene (dpb). **X-pcu-11-Zn** was found to undergo reversible structural transformations between its as-synthesized large pore "open" phase, **X-pcu-11-Zn-α**, and its activated narrow pore phase, **X-pcu-11-Zn-β**. These transformations were characterised by single-crystal X-ray diffraction (SCXRD) as well as gas and vapor adsorption to provide insight into the Bz binding mechanism.

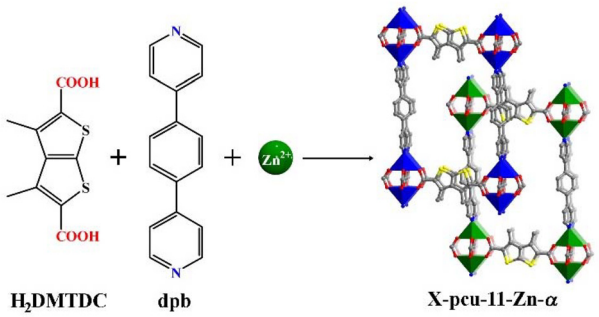

Scheme 1 **X-pcu-11-Zn-α** is composed of H_2DMTDC and dpb ligands and exhibits a primitive cubic (pcu) topology with 2-fold interpenetration.

Results and discussion

Synthesis and crystal structure

Solvothermal reaction of H_2DMTDC and dpb with Zn $(NO_3)_2{\cdot}6H_2O$ in DMF at 105 °C yielded colourless, block crystals of $[Zn_2(DMTDC)_2(dpb)]{\cdot}5DMF{\cdot}0.5H_2O$, **X-pcu-11-Zn-α** (full synthetic details are available in the ESI†). SCXRD revealed that **X-pcu-11-Zn-α** had crystallised in the triclinic space group $P\bar{1}$. The resulting coordination network comprises dinuclear Zn(II) tetracarboxylate paddlewheels (Fig. 1a) linked *via* DMTDC ligands to form a square lattice (**sql**) network (Fig. 1b). The **sql** nets are pillared by dpb linkers to generate a **pcu** topology (Fig. 1c). **X-pcu-11-Zn-α** is a member of the **DMOF-1** family which already has several members with extended (X-) ligands, **X-pcu-*n*-Zn** (*e.g.* n = 5, 6, 7, 8), that exhibit 2-fold offset interpenetration (Fig. 1d).[30–32] **X-pcu-11-Zn-α** features ultramicroporous 3D channels with effective pore diameters of *ca.* 2.3 × 2.5, 3.3 × 5.4, and 4.5 × 6.8 Å^2 along the *a*-, *b*-, and *c*-axes, respectively (Fig. S1–S3†). The calculated guest-accessible volume is 49.8%. TGA revealed that as-synthesized **X-pcu-11-Zn-α** loses guest molecules (observed:

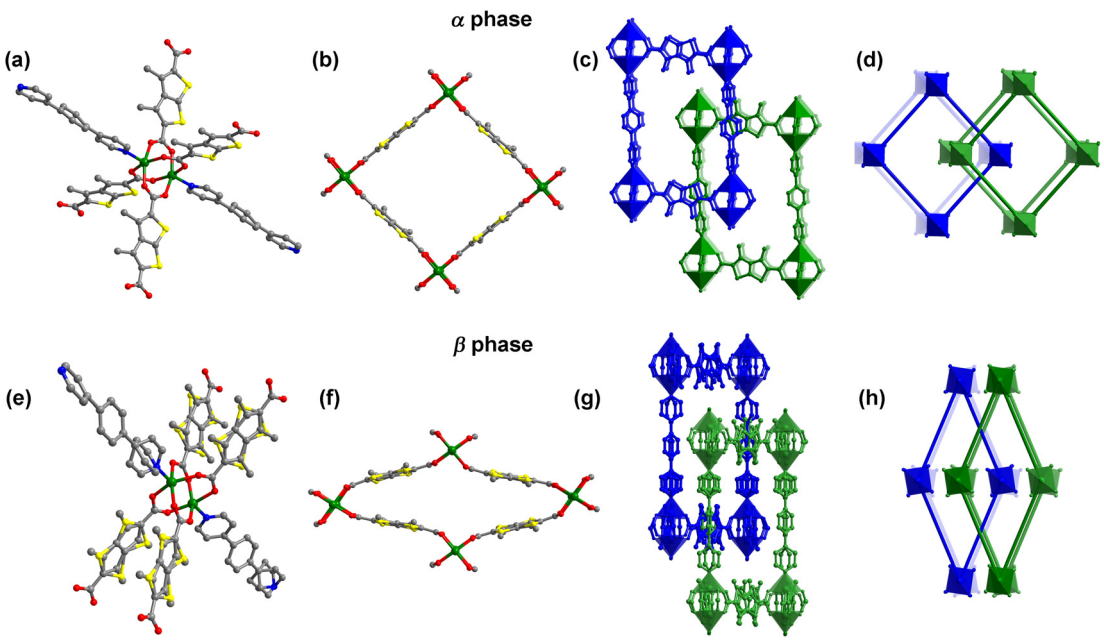

Fig. 1 Crystal structures of the α and β forms of **X-pcu-11-Zn** reveal zinc "paddlewheel" clusters (a and e), **sql** nets constructed by the clusters and DMTDC ligands (b and f), and two-fold interpenetrated structures (c, g, d and h). Hydrogen atoms are omitted for clarity. C (gray), Zn (green), O (red), N (blue), and S (yellow).

30.02%; calculated: 30.05%) on reaching 150 °C and is thermally stable below 320 °C (Fig. S8†).

X-pcu-11-Zn-α underwent single-crystal-to-single-crystal (SCSC) transformation after heating at 120 °C for 12 h to form **X-pcu-11-Zn-β** (Fig. S11†). SCXRD revealed that the β-form is a contorted version of the α-form with the same connectivity (Fig. 1e and f) but with centred rather than offset interpenetration (Fig. 1g). **X-pcu-11-Zn-β** crystallized in the orthorhombic space group *Ibca* with a 32.0% shrinkage in unit-cell volume relative to the α-form (Table S1†). **X-pcu-11-Zn-β** exhibits 1D channels with an effective pore diameter of *ca.* 2.1 × 2.6 Å^2 along the *a*-axis (Fig. S4†). TGA and IR studies indicated that guest molecules had indeed been removed (Fig. S8 and S10†) and PLATON calculations revealed that the β-phase has only 4.9% solvent-accessible space. TGA of **X-pcu-11-Zn-β** showed no weight loss until decomposition at 320 °C (Fig. S8†). The structural transformation associated with guest release is reversible, with PXRD data revealing that the β-form had reverted to the α-form when soaked in DMF at room temperature for one day (Fig. S11†).

Analysis of the crystal structures reveals that the transformation between the large pore and narrow pore phases involves distortion of the **sql** nets and a sliding motion of the two interpenetrated nets (Fig. 1 and Fig. S7, Table S2†). In the α-phase, the metal–carboxylate junction Zn2═O2 > C approaches linearity with dihedral angles (Table S2 and Fig. S5†) between the Zn2═O2 plane and the carboxylate group O2 > C ranging from 1.0° to 8.4° for **X-pcu-11-Zn-α**. Conversely, in the β-phase, the metal–carboxylate junctions bend with dihedral angles ranging from 18.1° to 30.1° for **X-pcu-11-Zn-β**. There are no π–π interactions (centroid–centroid distance <4.0 Å) or C–H-π interactions in either structure, but C–H···O hydrogen bonding exists in both phases (Table S3†).

Gas adsorption

That **X-pcu-11-Zn-β** was prepared from a large pore phase motivated us to determine if switching or breathing would occur when **X-pcu-11-Zn-α** is exposed to gases. As shown in Fig. 2, the β-form is nonporous to N_2 (kinetic diameter: 3.64 Å) at low pressure (P/P_0 < 0.1), consistent with its narrow pore dimensions (2.1 × 2.6 Å^2) and expected weak framework–N_2 interactions. β exhibited a 2-step adsorption profile for N_2 at 77 K, with saturation occurring after the second step. The first step, with an onset pressure of approximately P/P_0 = 0.10, is indicative of gas-induced gate-opening (switching) behaviour, suggesting a structural transformation from a non-porous phase to an intermediate pore phase. The resulting increase of overall pore volume at a threshold pressure of N_2 can result in a negative sorption step as seen in Fig. 2.[33] The intermediate phase existed until P/P_0 = 0.46. Upon further increasing the pressure to P/P_0 = 1.0, the framework transformed to the large pore α-form with an uptake of 337 cm^3 g^{-1}. The pore volume calculated by assuming liquid filling of saturated N_2 is 0.52 cm^3 g^{-1}, consistent with the void volume of **X-pcu-11-Zn-α** calculated from the crystal structure (0.50 cm^3 g^{-1}). These data suggest that **X-pcu-11-Zn-β** had reverted **X-pcu-11-Zn-α** under these sorption conditions. To the best of our knowledge, **X-pcu-11-Zn-β** is the first example of switching between closed and two open phases showing a two-step type F-IV^2 isotherm[8] (Table S7†) with high capacity (>300 cm^3 g^{-1}) although other switching sorbents exhibit one-step type F-IV^s isotherms (*e.g.* **DUT-8(Ni)**,[34] rtl-[Cu(HIsa-azdmpz)][35] and **ELM-11**[36]) or even a five-step type F-IV^5 isotherm (Co(bpe)) with an uptake >300 cm^3 g^{-1}.[37]

Unlike N_2 adsorption at 77 K, the adsorption isotherm of CO_2 for **X-pcu-11-Zn-β** at 195 K consists of three adsorption/desorption steps. The initial uptake of CO_2 reached a saturated uptake of 33 cm^3 g^{-1}. The Langmuir surface area calculated for the first CO_2 sorption step is 200 m^2 g^{-1}. The next step, which we attribute to gate-opening, occurred at P/P_0 = 0.10 with saturated uptake reaching 125 cm^3 g^{-1}. The Langmuir surface area calculated from the second-step of CO_2 sorption is 754 m^2 g^{-1}. At the second gate-opening pressure (P/P_0 = 0.70), the CO_2 uptake further increased to 267 cm^3 g^{-1} at P/P_0 = 1.0. The Langmuir surface area was calculated to be 1677 m^2 g^{-1} (see section 10†).[38] **X-pcu-11-Zn-β** represents a rare example of 3-step CO_2 adsorption with high capacity (>250 cm^3 g^{-1}) (Table S8†). After N_2 and CO_2 desorption, **X-pcu-11-Zn-β** retained its original structure (Fig. S12†).

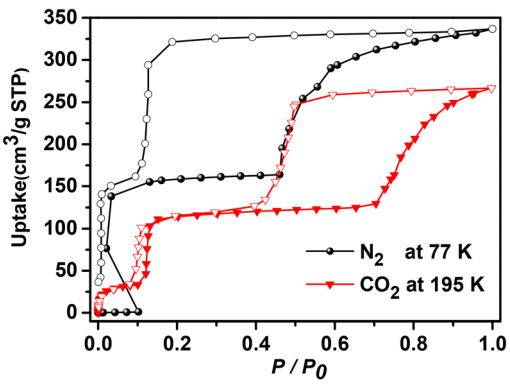

Fig. 2 Gas sorption isotherms of **X-pcu-11-Zn-β**. Solid and open symbols represent adsorption and desorption branches, respectively.

Vapour sorption

Dynamic vapour sorption measurements were conducted at 298 K to further study the dynamic properties of **X-pcu-11-Zn-β**. Fig. 3 illustrates the adsorption/desorption isotherms of **X-pcu-11-Zn-β** for H_2O, MeOH, EtOH and CH_3CN at 298 K. **X-pcu-11-Zn-β** preferentially adsorbed aliphatic organic molecules over water vapor despite the smaller kinetic diameter of H_2O compared to that of the organic molecules. For MeOH and EtOH, gate-opening pressures were found to be P/P_0 = 0.7 for MeOH and 0.6 for EtOH, with uptakes of 211 and 140 cm^3 g^{-1}, respectively, at P/P_0 = 0.96. In contrast, the isotherm for CH_3CN shows a 3-step adsorption process, with gate-opening pressures at P/P_0 = 0.18 and 0.66, and an uptake of 194 cm^3 g^{-1} at P/P_0 = 0.96. These gate-opening phenomena are consistent with guest-induced structural transformations for MeOH, EtOH and

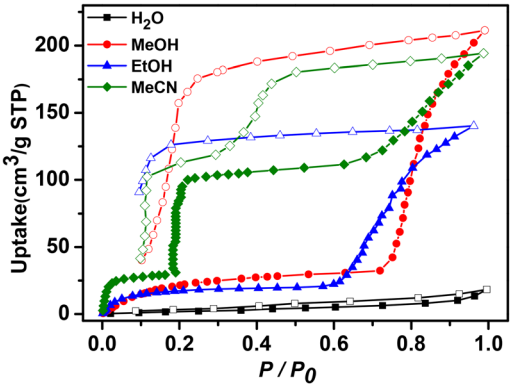

Fig. 3 H_2O, MeOH, EtOH, and MeCN sorption isotherms measured at 298 K. Solid and open symbols represent adsorption and desorption branches, respectively.

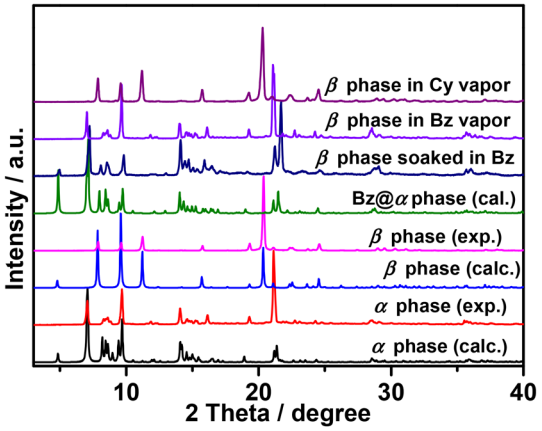

Fig. 5 PXRD patterns of **X-pcu-11-Zn** under different conditions.

CH_3CN, whereas H_2O did not induce such transformations (Fig. S13†), indicating that **X-pcu-11-Zn** is hydrophobic.

To investigate the adsorption behaviour of larger organic molecules on **X-pcu-11-Zn-β**, single-component adsorption isotherms for benzene (Bz) and cyclohexane (Cy) were collected at 298 K. As shown in Fig. 4, **X-pcu-11-Zn-β** adsorbed Bz (92 cm^3 g^{-1}) but exhibited minimal adsorption for Cy (5 cm^3 g^{-1}) at P/P_0 = 0.99. This uptake amount corresponds to 3.56 Bz molecules per formula unit. Although Bz is larger than MeOH, EtOH, and MeCN, its gate-opening adsorption pressure starts at a lower relative pressure (P/P_0 = 0.10), which may be attributed to host–guest interactions arising from the π system and the more acidic C(sp^2)–H moieties in Bz compared to C(sp^3)–H bonds. PXRD patterns of **X-pcu-11-Zn-β** exposed to Bz for 12 h reveal distinct changes compared to the patterns of unexposed **X-pcu-11-Zn-β**, whereas the PXRD patterns remained unchanged under Cy vapour for the same duration (Fig. 5). PXRD data suggest that the structure of **X-pcu-11-Zn-β** after exposure to Bz for 12 h matches well with that of **X-pcu-11-Zn-α** calculated from SCXRD data, indicating that Bz had induced structural transformation from the β to the α phase, while Cy did not induce such a change (Fig. 5). This makes **X-pcu-11-Zn-β** a candidate for selective adsorption of Bz over Cy.

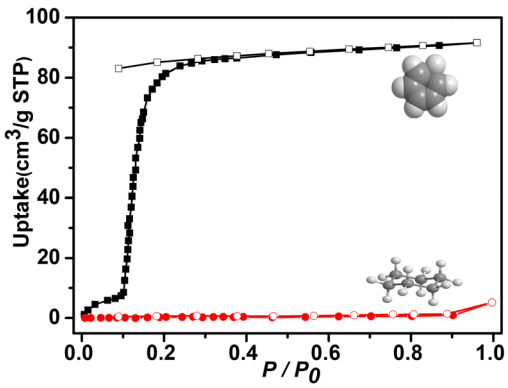

Fig. 4 Bz and Cy sorption isotherms measured at 298 K.

To gain insight into this adsorption behaviour, single crystals of **Bz@X-pcu-11-Zn** were obtained by soaking **X-pcu-11-Zn-α** in benzene (Bz). PXRD analyses indicate that Bz-loaded **X-pcu-11-Zn** is indeed isostructural with **X-pcu-11-Zn-α** as calculated from SCXRD data (Fig. 5). The single crystal structure of Bz-loaded **X-pcu-11-Zn** reveals the presence of 3.5 Bz molecules per molecular unit, consistent with the uptake from the Bz adsorption isotherm. In the crystal structure of **Bz@X-pcu-11-Zn**, the framework resembles that of **X-pcu-11-Zn-α** with similar unit cell parameters (Table S1†). As shown in Fig. 6 and Tables S4, S5,† multiple π–π and C–H···π aromatic interactions exist between the benzene molecules and the **X-pcu-11-Zn** framework, which likely drive the phase transformation of **X-pcu-11-Zn-β**. The selectivity of **X-pcu-11-Zn-β** for Bz can be attributed to this host–guest binding. Furthermore, the PXRD pattern of **X-pcu-11-Zn-β** after Bz capture also matches well with the calculated pattern from the crystal structure of **Bz@X-**

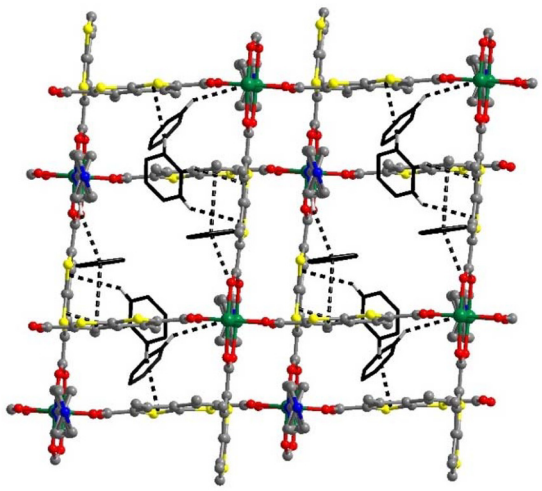

Fig. 6 The π···π and C–H···π interactions between benzene molecules and the framework in **Bz@X-pcu-11-α** viewed along the crystallographic *b*-axis.

pcu-11-Zn- (Fig. 5), indicating that the crystal structure transforms from **X-pcu-11-Zn-β** to **Bz@X-pcu-11-Zn** upon Bz adsorption. The ^{1}H NMR spectra of **X-pcu-11-Zn-β** exposed to Bz and Cy vapours for 12 h showed that **X-pcu-11-Zn-β** adsorbs 3.48 Bz and 0.04 Cy molecules per molecular unit (Fig. S19 and S20†), respectively. Additionally, TGA data were collected for Bz and Cy vapour adsorption by **X-pcu-11-Zn-β**. As shown in Fig. S9,† the TGA curves for **X-pcu-11-Zn-β** that had been exposed to Bz for 12 h reveal a weight loss of 22.61% below 115 °C, corresponding to 3.26 Bz molecules per molecular unit, again consistent with the SCXRD analysis results. In contrast, there is negligible weight loss (2.61%) for **X-pcu-11-Zn-β** after exposure to Cy vapor for 12 h before reaching 300 °C. This pronounced adsorption difference suggested to us that **X-pcu-11-Zn-β** can be utilised for the separation of Bz and Cy.

To evaluate the adsorption kinetics of **X-pcu-11-Zn-β** for benzene (Bz) and cyclohexane (Cy) vapours, ^{1}H NMR spectroscopy was employed (details are available in the ESI†). Samples that had been exposed to Bz and Cy vapours were soaked in $CDCl_3$ to extract adsorbed Bz and Cy, respectively. As depicted in Fig. 7a, the amount of Bz adsorbed by **X-pcu-11-Zn-β** increased over time, reaching saturation after approximately 1 h at room temperature. At saturation, **X-pcu-11-Zn-β** adsorbed about 3.48 Bz molecules per unit, while the uptake of Cy was negligible. The adsorption kinetics for Bz were analysed by using pseudo-first-order and pseudo-second-order kinetic models (see section 15 of the ESI†). As shown in Fig. S23, S24 and Table S6,† the adsorption kinetics can be best described by the pseudo-first-order model for **X-pcu-11-Zn-β**. This suggests that the adsorption process may be governed by physisorption rather than chemisorption. The structural changes induced by Bz adsorption were found to be reversible; adsorbed Bz was removed by heating **Bz@X-pcu-11-Zn** at 120 °C under vacuum (Fig. S14†). So-formed **X-pcu-11-Zn-β** retained its ability to adsorb Bz with no loss of performance after six cycles (Fig. 7b) and PXRD data revealed that **X-pcu-11-Zn-β** maintained phase stability (Fig. S14†).

To explore the potential of **X-pcu-11-Zn-β** for separating Bz and Cy mixtures, a time-dependent binary-component sorption experiment was conducted with **X-pcu-11-Zn-β** exposed to an equimolar Bz/Cy vapor mixture (details are available in the ESI†). In contrast to single-component adsorption, binary-component Bz/Cy adsorption resulted in co-adsorption, 2.10 Bz and 0.97 Cy molecules per formula unit, respectively, after 12 h of exposure to equimolar Bz/Cy (Fig. 7c). The separation ratio of the Bz/Cy mixture was calculated to be 2.16. Although the Bz/Cy selectivity is smaller than other flexible MOFs (Table S9†) such as $[Zn(TCNQ\text{-}TCNQ)bpy]_n$ [26] and CID-23,[39] this value is comparable or better than several rigid MOFs such as MOF-5,[40] HKUST-1,[41] and CUB-30.[42] Binary-component Bz/Cy adsorption by gas chromatography revealed that **X-pcu-11-Zn-β** reached saturation for Bz and Cy within 1 h (Fig. S22†), and had adsorbed 76.52% Bz and 23.48% Cy after 1 h (Fig. 7d). The molar ratio of Bz/Cy (3.2 : 1) from gas chromatography is comparable to that obtained from ^{1}H NMR analyses. As expected, the PXRD pattern of **X-pcu-11-Zn-β** changed upon exposure to the Bz/Cy mixture, matching the calculated pattern from the SCXRD data of **Bz@X-pcu-11-Zn** (Fig. S15†). These results indicate that **X-pcu-11-Zn-β** is a soft crystalline material with moderate selectivity for adsorption of Bz from a 1 : 1 Bz/Cy mixture, the selectivity being ascribed to the structural transformation induced by Bz adsorption.

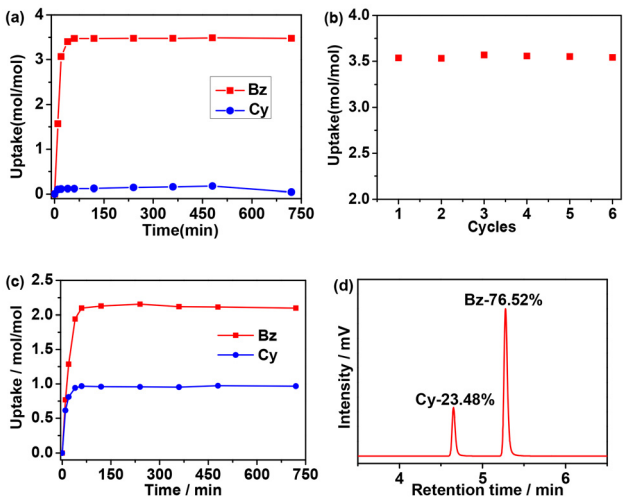

Fig. 7 (a) Time-dependent single-component solid–vapour sorption plots of **X-pcu-11-Zn-β** under ambient conditions; (b) the uptake of Bz by **X-pcu-11-Zn-β** after 6 recycles; (c) time-dependent binary-component solid–vapour adsorption plots of **X-pcu-11-Zn-β** in Bz/Cy equimolar mixture vapour according to ^{1}H-NMR spectroscopy data; and (d) gas chromatography of **X-pcu-11-Zn-β** in equimolar Bz and Cy mixtures for 1 h.

Conclusions

In summary, we report a flexible, 2-fold interpenetrated coordination network, **X-pcu-11-Zn**, with π-conjugated thiophene-containing dicarboxylate and benzene-bridged bipyridine ligands. **X-pcu-11-Zn** exhibited reversible structural transformations between large pore and narrow pore phases. For N_2 adsorption, a 2-step N_2 F-IV[2] isotherm at 77 K was observed with an uptake of 337 $cm^3\ g^{-1}$. A 3-step CO_2 sorption isotherm was observed at 195 K with the uptake exceeding 260 $cm^3\ g^{-1}$. To our knowledge, **X-pcu-11-Zn** is the first example of switching between closed and two open phases showing a two-step F-IV[2] isotherm with high capacity (>300 $cm^3\ g^{-1}$). Vapor sorption experiments revealed that **X-pcu-11-Zn** is selective for methanol, ethanol, and CH_3CN over H_2O, characterized by stepped vapour sorption isotherms and significant hysteresis. Most notably, it selectively adsorbs Bz over Cy, with gate-opening concomitant with structural transformations. The transformations between the guest-free and guest-containing structures are reversible, with **X-pcu-11-Zn** maintaining its ability to adsorb benzene without performance loss after six cycles. SCXRD studies indicated that the selective adsorption is driven by host–guest interactions, including multiple π–π and C–H···π aromatic interactions, which induce structural

transformation and gate-opening upon benzene sorption. This study highlights that two-fold interpenetrated flexible MOFs with π-conjugated ligands, which have many possible variants, offer potential to selectively adsorb/separate Bz over Cy driven by Bz-selective binding sites.

Data availability

The data supporting the findings of this study are available in the ESI† or from the authors upon request.

Conflicts of interest

The authors declare no competing financial interest.

Acknowledgements

This work was financially supported by the National Natural Science Foundation of China (no. 22161052) and Research Ireland (SFI award 16/IA/4624). We also thank Ji-Kai Chen and Sheng-Ming Xie (Yunnan Normal University) for gas chromatography testing.

References

1 L. R. MacGillivray, *Metal-organic frameworks: design and application*, John Wiley & Sons, 2010.
2 S. Kitagawa, R. Kitaura and S. Noro, Functional Porous Coordination Polymers, *Angew. Chem., Int. Ed.*, 2004, **43**, 2334–2375.
3 Z. R. Herm, E. D. Bloch and J. R. Long, Hydrocarbon Separations in Metal-Organic Frameworks, *Chem. Mater.*, 2014, **26**, 323–338.
4 S. Horike, S. Shimomura and S. Kitagawa, Soft porous crystals, *Nat. Chem.*, 2009, **1**, 695–704.
5 A. Schneemann, V. Bon, I. Schwedler, I. Senkovska, S. Kaskel and R. A. Fischer, Flexible metal-organic frameworks, *Chem. Soc. Rev.*, 2014, **43**, 6062–6096.
6 R. F. Mendes and F. A. A. Paz, Transforming metal-organic frameworks into functional materials, *Inorg. Chem. Front.*, 2015, **2**, 495–509.
7 J. H. Lee, S. Jeoung, Y. G. Chung and H. R. Moon, Elucidation of flexible metal-organic frameworks: Research progresses and recent developments, *Coord. Chem. Rev.*, 2019, **389**, 161–188.
8 S. Q. Wang and S. M. J. Zaworotko, Spiers Memorial Lecture: Coordination networks that switch between nonporous and porous structures: an emerging class of soft porous crystals, *Faraday Discuss.*, 2021, **231**, 9–50.
9 X. Yao, K. E. Cordova and Y.-B. Zhang, Flexible Metal-Organic Frameworks as CO_2 Adsorbents en Route to Energy-Efficient Carbon Capture, *Small Struct.*, 2022, **3**, 2100209.
10 M. K. Taylor, T. Runcevski, J. Oktawiec, J. E. Bachman, R. L. Siegelman, H. Jiang, J. A. Mason, J. D. Tarver and J. R. Long, Near-Perfect CO_2/CH_4 Selectivity Achieved through Reversible Guest Templating in the Flexible Metal-Organic Framework Co(bdp), *J. Am. Chem. Soc.*, 2018, **140**, 10324–10331.
11 Y. Li, Y. Wang, W. Fan and D. Sun, Flexible metal-organic frameworks for gas storage and separation, *Dalton Trans.*, 2022, **51**, 4608–4618.
12 Z. Chang, D.-H. Yang, J. Xu, T.-L. Hu and X.-H. Bu, Flexible Metal-Organic Frameworks: Recent Advances and Potential Applications, *Adv. Mater.*, 2015, **27**, 5432–5441.
13 N. Yanai, K. Kitayama, Y. Hijikata, H. Sato, R. Matsuda, Y. Kubota, M. Takata, M. Mizuno, T. Uemura and S. Kitagawa, Gas detection by structural variations of fluorescent guest molecules in a flexible porous coordination polymer, *Nat. Mater.*, 2011, **10**, 787–793.
14 J.-H. Wang, M. Li and D. Li, A dynamic, luminescent and entangled MOF as a qualitative sensor for volatile organic solvents and a quantitative monitor for acetonitrile vapour, *Chem. Sci.*, 2013, **4**, 1793–1801.
15 A. Douvali, A. C. Tsipis, S. V. Eliseeva, S. Petoud, G. S. Papaefstathiou, C. D. Malliakas, I. Papadas, G. S. Armatas, I. Margiolaki, M. G. Kanatzidis, T. Lazarides and M. J. Manos, Turn-On Luminescence Sensing and Real-Time Detection of Traces of Water in Organic Solvents by a Flexible Metal–Organic Framework, *Angew. Chem., Int. Ed.*, 2015, **54**, 1651–1656.
16 K. Koupepidou, A. Subanbekova and M. J. Zaworotko, Functional flexible adsorbents and their potential utility, *Chem. Commun.*, 2025, **61**, 3109–3126.
17 S. Mukherjee, D. Sensharma, O. T. Qazvini, S. Dutta, L. K. Macreadie, S. K. Ghosh and R. Babarao, Advances in adsorptive separation of benzene and cyclohexane by metal-organic framework adsorbents, *Coord. Chem. Rev.*, 2021, **437**, 213852.
18 Z. Zhang, S. B. Peh, C. Kang, K. Chai and D. Zhao, Metal-organic frameworks for C6-C8 hydrocarbon separations, *EnergyChem*, 2011, **3**, 100057.
19 J. Qin, Q. Ye, X. Xiong and N. Li, Control of Benzene-Cyclohexane Separation System via Extractive Distillation Using Sulfolane as Entrainer, *Ind. Eng. Chem. Res.*, 2013, **52**, 10754–10766.
20 P. Navarro, A. Ovejero-Pérez, M. Ayusob, N. Delgado-Mellado, M. Larriba, J. García and F. Rodríguez, Cyclohexane/cyclohexene separation by extractive distillation with cyano-based ionic liquids, *J. Mol. Liq.*, 2019, **289**, 111120.
21 M. Ayuso, A. Cañada-Barcala, M. Larriba, P. Navarro, N. Delgado-Mellado, J. Garía and F. Rodríguez, Enhanced separation of benzene and cyclohexane by homogeneous extractive distillation using ionic liquids as entrainers, *Sep. Purif. Technol.*, 2020, **240**, 116583.
22 M. Shivanna, K. Otake, B.-Q. Song, L. M. van Wyk, Q.-Y. Yang, N. Kumar, W. K. Feldmann, T. Pham, S. Suepaul, B. Space, L. J. Barbour, S. Kitagawa and

M. J. Zaworotko, Benchmark Acetylene Binding Affinity and Separation through Induced Fit in a Flexible Hybrid Ultramicroporous Material, *Angew. Chem., Int. Ed.*, 2021, **60**, 20383–20390.

23 Z.-C. Xu, J. Yu, P.-D. Zhang, Y.-L. Zhao, X.-Q. Wu, M. Zhao, X. Zhang and J.-R. Li, Efficient C_2H_2 Separation from CO_2 and CH_4 within a Microporous Metal-Organic Framework of Multiple Functionalities, *Ind. Eng. Chem. Res.*, 2022, **61**, 16233–16239.

24 H. Yao, Y.-M. Wang, M. Quan, M. U. Farooq, L.-P. Yang and W. Jiang, Adsorptive Separation of Benzene, Cyclohexene, and Cyclohexane by Amorphous Nonporous Amide Naphthotube Solids, *Angew. Chem., Int. Ed.*, 2020, **59**, 19945–19950.

25 J. Zhou, G. Yu, Q. Li, M. Wang and F. Huang, Separation of Benzene and Cyclohexane by Nonporous Adaptive Crystals of a Hybrid[3]arene, *J. Am. Chem. Soc.*, 2020, **142**, 2228–2232.

26 S. Shimomura, S. Horike, R. Matsuda and S. Kitagawa, Guest-Specific Function of a Flexible Undulating Channel in a 7,7,8,8-Tetracyano-p-quinodimethane Dimer-Based Porous Coordination Polymer, *J. Am. Chem. Soc.*, 2007, **129**, 10990–10991.

27 J.-P. Zhang and X.-M. Chen, Exceptional Framework Flexibility and Sorption Behavior of a Multifunctional Porous Cuprous Triazolate Framework, *J. Am. Chem. Soc.*, 2008, **130**, 6010–6017.

28 B. Joarder, S. Mukherjee, A. K. Chaudhari, A. V. Desai, B. Manna and S. K. Ghosh, Guest-Responsive Function of a Dynamic Metal-Organic Framework with a π Lewis Acidic Pore Surface, *Chem. – Eur. J.*, 2014, **20**, 15303–15308.

29 A. Karmakar, A. V. Desai, B. Manna, B. Joarder and S. K. Ghosh, An Amide-Functionalized Dynamic Metal-Organic Framework Exhibiting Visual Colorimetric Anion Exchange and Selective Uptake of Benzene over Cyclohexane, *Chem. – Eur. J.*, 2015, **21**, 7071–7076.

30 D. N. Dybtsev, H. Chun and K. Kim, Rigid and Flexible: A Highly Porous Metal-Organic Framework with Unusual Guest-Dependent Dynamic Behavior, *Angew. Chem., Int. Ed.*, 2004, **43**, 5033–5036.

31 A.-X. Zhu, Q.-Y. Yang, A. Kumar, C. Crowley, S. Mukherjee, K.-J. Chen, S.-Q. Wang, D. O'Nolan, M. Shivanna and M. J. Zaworotko, Coordination Network That Reversibly Switches between Two Nonporous Polymorphs and a High Surface Area Porous Phase, *J. Am. Chem. Soc.*, 2018, **140**, 15572–15576.

32 A.-X. Zhu, Q.-Y. Yang, S. Mukherjee, A. Kumar, C.-H. Deng, A. A. Bezrukov, M. Shivanna and M. J. Zaworotko, Tuning the Gate-Opening Pressure in a Switching pcu Coordination Network, X-pcu-5-Zn, by Pillar-Ligand Substitution, *Angew. Chem., Int. Ed.*, 2019, **58**, 18212–18217.

33 Y.-X. Shi, W.-X. Li, W.-H. Zhang and J.-P. Lang, Guest-Induced Switchable Breathing Behavior in a Flexible Metal–Organic Framework with Pronounced Negative Gas Pressure, *Inorg. Chem.*, 2018, **57**, 8627–8633.

34 N. Klein, H. C. Hoffmann, A. Cadiau, J. Getzschmann, M. R. Lohe, S. Paasch, T. Heydenreich, K. Adil, I. Senkovska, E. Brunner and S. Kaskel, Structural flexibility and intrinsic dynamics in the M2(2,6-ndc)2(dabco) (M = Ni, Cu, Co, Zn) metal-organic frameworks, *J. Mater. Chem.*, 2012, **22**, 10303–10312.

35 S. Millan, B. Gil-Hernández, E. Milles, S. Gökpinar, G. Makhloufi, A. Schmitz, C. Schlüsenera and C. Janiak, rtl-M-MOFs (M = Cu, Zn) with a T-shaped bifunctional pyrazole-isophthalate ligand showing flexibility and S-shaped Type F-IV sorption isotherms with high saturation uptakes for M = Cu, *Dalton Trans.*, 2019, **48**, 8057–8067.

36 H. Noguchi, A. Kondo, Y. Hattori, H. Kajiro, H. Kanoh and K. Kaneko, Evaluation of an Effective Gas Storage Amount of Latent Nanoporous Cu-Based Metal-Organic Framework, *J. Phys. Chem. C*, 2007, **111**, 248–254.

37 H. J. Choi, M. Dinca and J. R. Long, Broadly Hysteretic H2 Adsorption in the Microporous Metal-Organic Framework Co(1,4-benzenedipyrazolate), *J. Am. Chem. Soc.*, 2008, **130**, 7848–7850.

38 L.-H. Xie and M. P. Suh, Flexible Metal-Organic Framework with Hydrophobic Pores, *Chem. – Eur. J.*, 2011, **17**, 13653–13656.

39 Y. Hijikata, S. Horike, M. Sugimoto, H. Sato, R. Matsuda and S. Kitagawa, Relationship between Channel and Sorption Properties in Coordination Polymers with Interdigitated Structures, *Chem. – Eur. J.*, 2011, **17**, 5138–5144.

40 M. Eddaoudi, H. Li and O. M. Yaghi, Highly Porous and Stable Metal-Organic Frameworks: Structure Design and Sorption Properties, *J. Am. Chem. Soc.*, 2000, **122**, 1391–1397.

41 F.-J. Ma, S.-X. Liu, D.-D. Liang, G.-J. Ren, F. Wei, Y.-G. Chen and Z.-M. Su, Adsorption of volatile organic compounds in porous metal-organic frameworks functionalized by polyoxometalates, *J. Solid State Chem.*, 2011, **184**, 3034–3039.

42 L. K. Macreadie, R. Babarao, C. J. Setter, S. J. Lee, O. T. Qazvini, A. J. Seeber, J. Tsanaktsidis, S. G. Telfer, S. R. Batten and M. R. Hill, Enhancing Multicomponent Metal-Organic Frameworks for Low Pressure Liquid Organic Hydrogen Carrier Separations, *Angew. Chem., Int. Ed.*, 2020, **59**, 6090–6098.